CHEMISTRY
AN ASIAN JOURNAL

Supporting Information

MIL-53(Al) as a Versatile Platform for Ionic-Liquid/MOF Composites to Enhance CO_2 Selectivity over CH_4 and N_2

Safiyye Kavak[+,[a, c]] H. Mert Polat[+,[a, c]] Harun Kulak[+,[b, c]] Seda Keskin,*[b, c] and Alper Uzun*[b, c, d]

asia_201900634_sm_miscellaneous_information.pdf

Table S1. Physical and chemical properties of the MOFs we considered in this work.

MOF	Metal	Organic Ligand	Surface Area (m^2/g)	Pore Volume (cm^3/g)	Hydro (philicity/phobicity)	Exposed Adsorption Sites
MIL-53(Al)	Al^{3+}	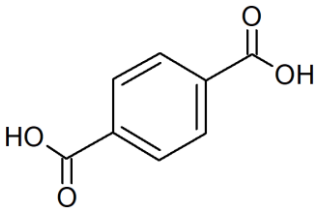	472	0.161	Hydrophilic	Exposed hydroxyl bridges (μ_2(O−H))
CuBTC	Cu^{2+}	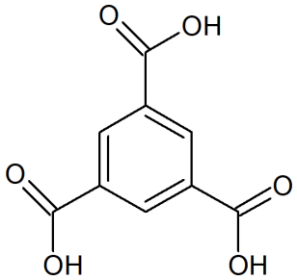	1324[1]	0.522[1]	Hydrophilic	Open metal site
ZIF-8	Zn^{2+}	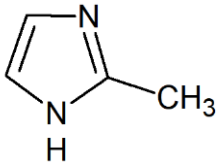	1208[2]	0.633[2]	Hydrophobic	None

Table S2. Physical and chemical properties of the ILs we considered in this work.

IL	Anion Structure	Molecular Formula	Molecular Weight (g/mol)	Hydro (philicity/phobicity)
[BMIM][BF_4]	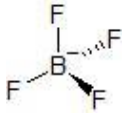	$C_8H_{15}BF_4N_2$	226.02	Hydrophilic
[BMIM][PF_6]	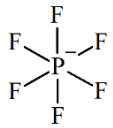	$C_8H_{15}F_6N_2P$	284.18	Hydrophobic
[BMIM][CF_3SO_3]	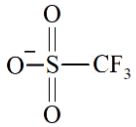	$C_9H_{15}F_3N_2O_3S$	288.29	Hydrophilic
[BMIM][SbF_6]	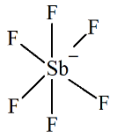	$C_8F_6H_{15}N_2Sb$	374.97	Hydrophobic
[BMIM][$MeSO_4$]	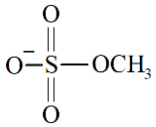	$C_9H_8N_2O_4S$	250.32	Hydrophilic
[BMIM][NTf_2]	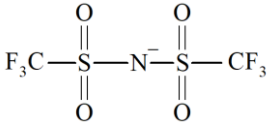	$C_{10}H_{15}F_6N_3O_4S_2$	419.36	Hydrophobic

Table S3. Densities, calculated loading of ILs (wt.% and vol.%), the corresponding pore filling degrees, and the number of IL molecules per unit cell of MIL-53(Al) in the composites prepared.

	Density of IL (g/cm^3)	**IL loading (wt.%)**	**IL loading (vol.%)**	**Pore filling Degree (%)**	**# of IL molecules/unit cell of MIL-53(Al)**
[BMIM][BF_4]/ MIL-53(Al)	1.21	25.8	21.4	77	1.22
[BMIM][PF_6]/ MIL-53(Al)	1.38	25.4	19	69	0.97
[BMIM][CF_3SO_3]/ MIL-53(Al)	1.29	25.8	20.3	63	0.98
[BMIM][SbF_6]/ MIL-53(Al)	NA	26	–	65	0.76
[BMIM][NTf_2]/ MIL-53(Al)	1.43	24.1	17.5	59	0.62

Number of ion pairs per unit cell in composites are calculated using IL-loading calculated from XRF and ICP-MS, molecular weight of ILs, crystal density of MIL-53(Al) (0.955 g/cm^3) and unit cell volume (6.6085 × 16.675 × 12.813 $Å^3$) from corresponding The Cambridge Structural Database (CSD)[3] entry (Refcode: SABVUN[4]).

Brunauer−Emmett−Teller (BET) Surface Area

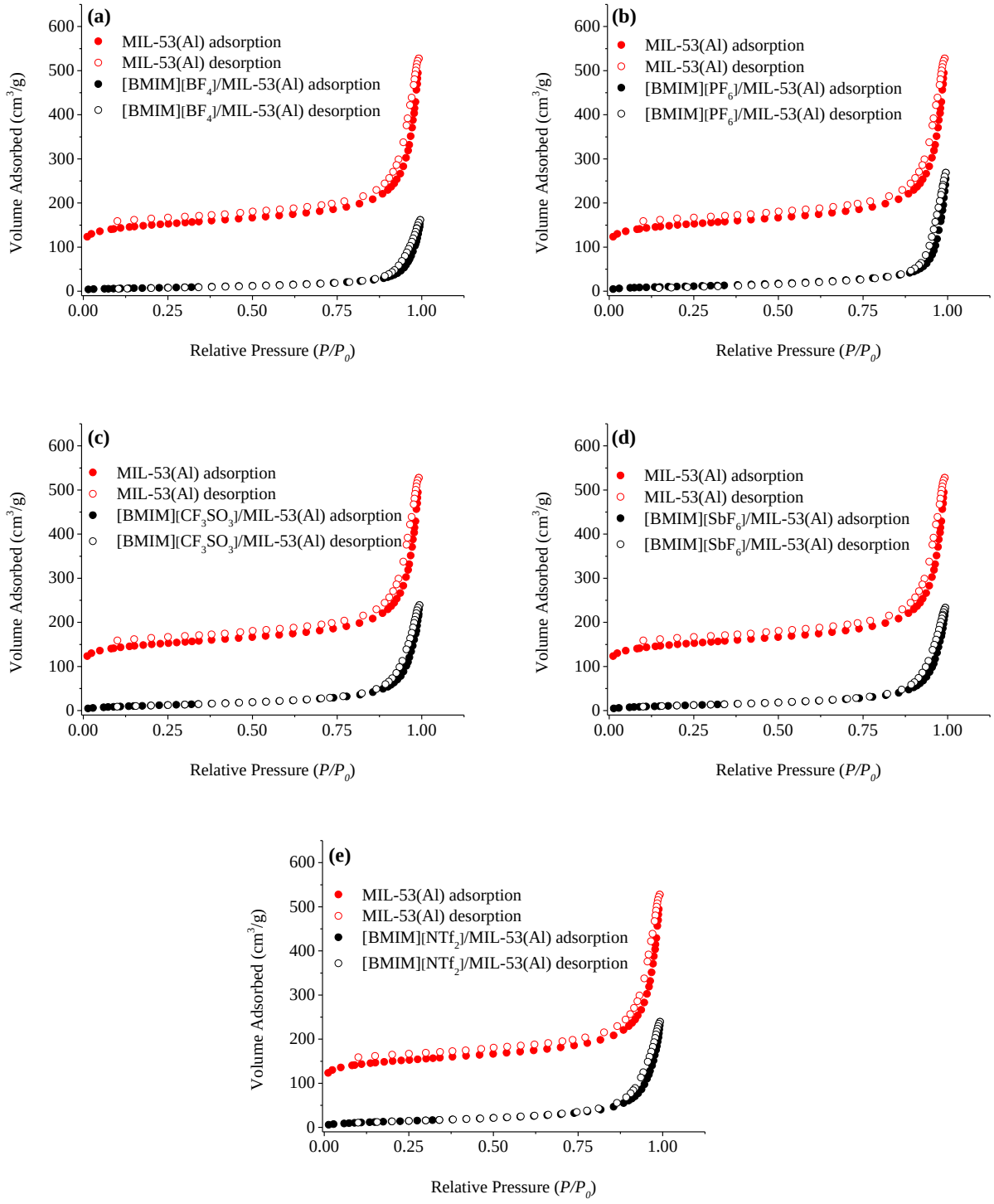

Figure S1. N_2 adsorption-desorption isotherms of pristine MIL-53(Al), and **(a)** [BMIM][BF_4]/MIL-53(Al), **(b)** [BMIM][PF_6]/MIL-53(Al), **(c)** [BMIM][CF_3SO_3]/MIL-53(Al), **(d)** [BMIM][SbF_6]/MIL-53(Al), and **(e)** [BMIM][NTf_2]/MIL-53(Al).

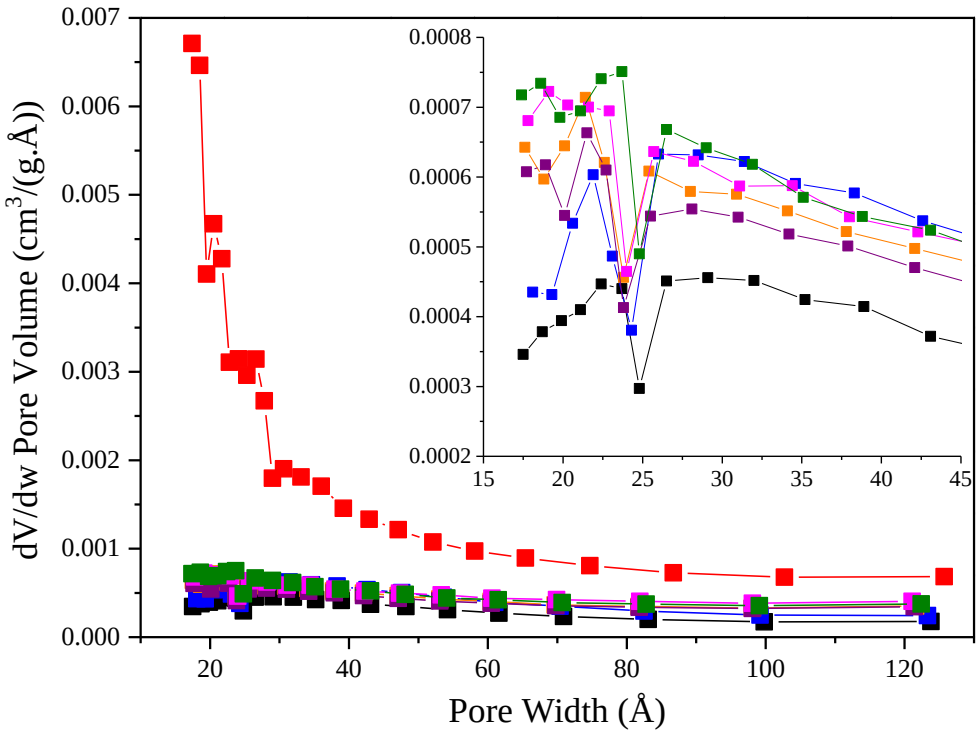

Figure S2. Pore size distribution (PSD) for MIL-53(Al) and all IL/MIL-53(Al) samples. Color code: red, MIL-53(Al); black, [BMIM][BF_4]/MIL-53(Al); blue, [BMIM][PF_6]/MIL-53(Al); orange, [BMIM][CF_3SO_3]/MIL-53(Al); violet, [BMIM][SbF_6]/MIL-53(Al); olive, [BMIM][$MeSO_4$]/MIL-53(Al); pink, [BMIM][NTf_2]/MIL-53(Al). The inset graph shows a zoomed-in view of the IL/MIL-53(Al) samples for a clearer representation of the PSD between 15-45 Å.

Scanning Electron Microscopy (SEM)

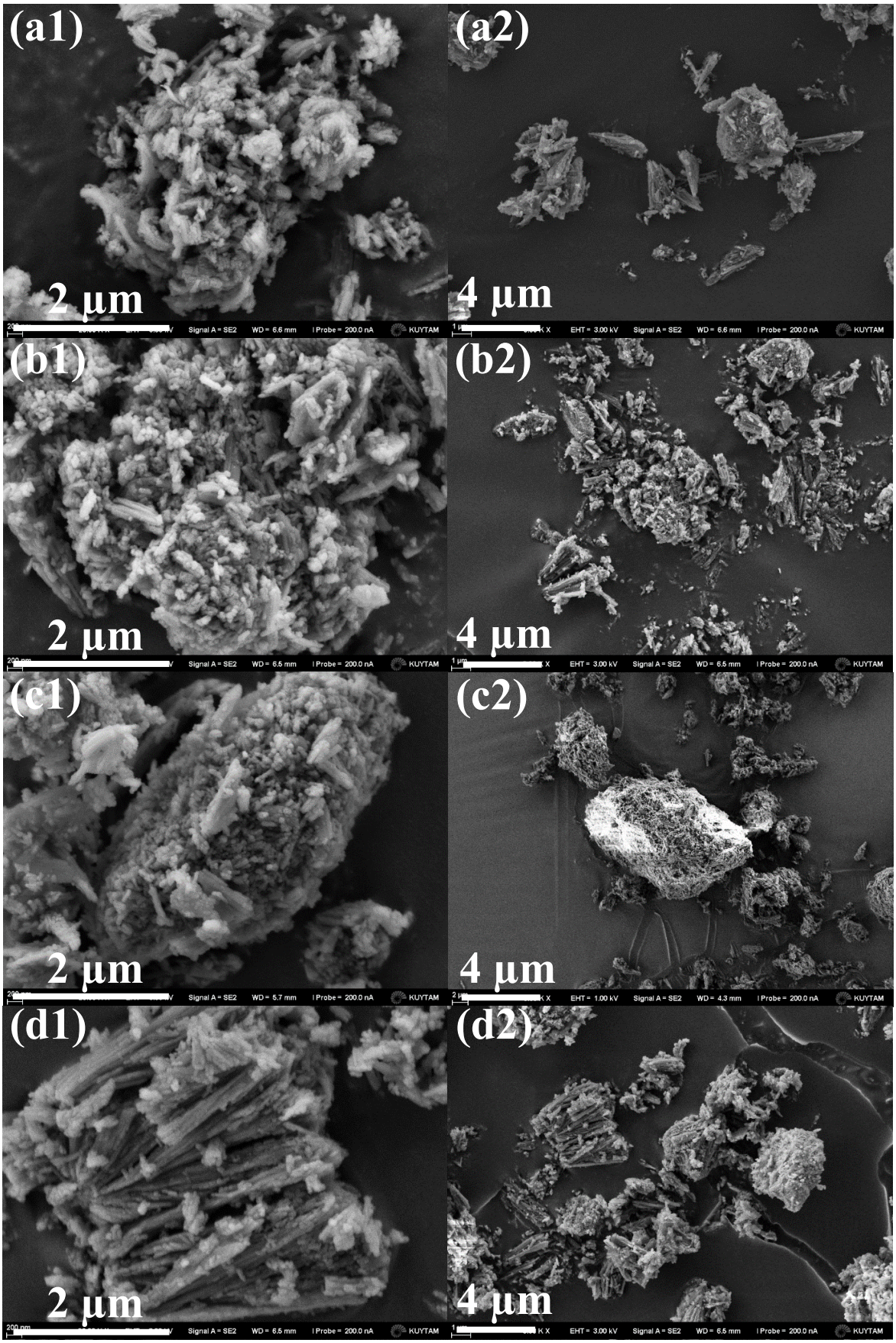

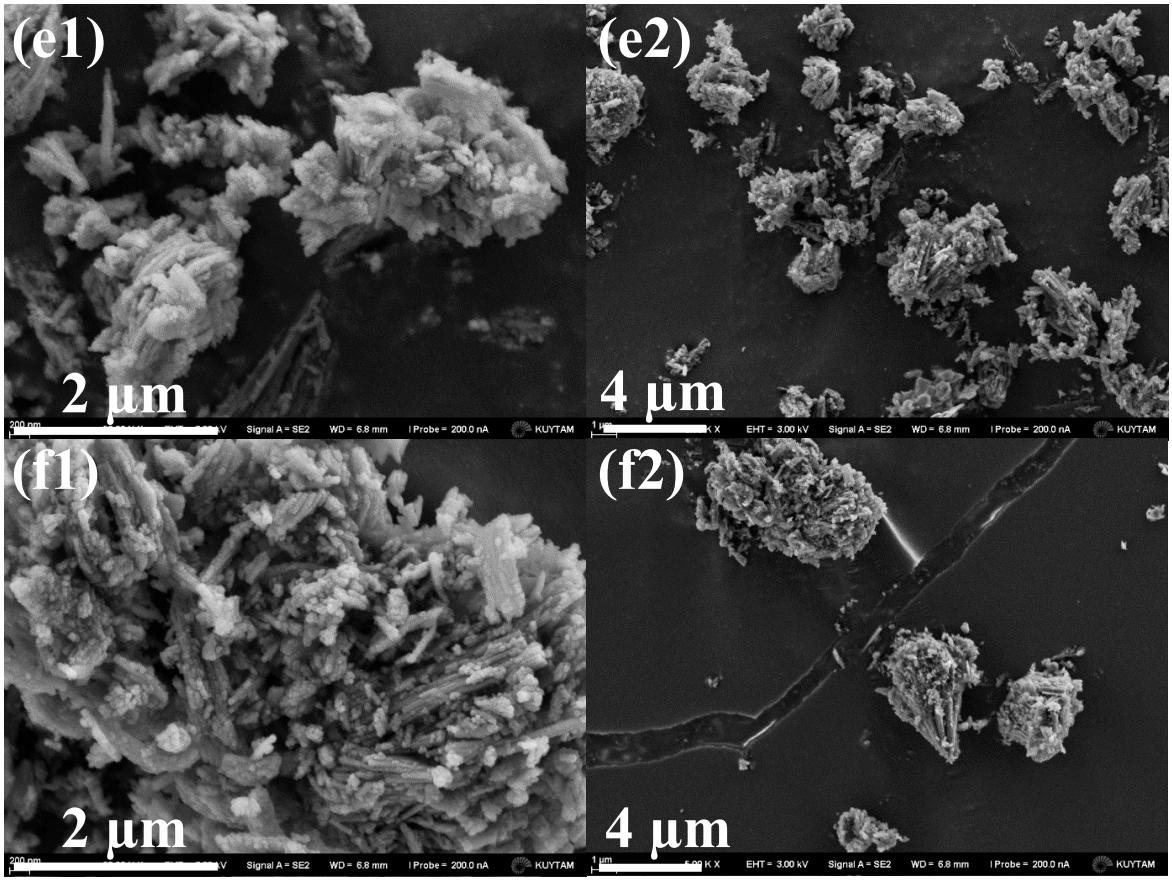

Figure S3. Additional SEM images of **(a)** pristine MIL-53(Al), **(b)** [BMIM][BF_4]/MIL-53(Al), **(c)** [BMIM][PF_6]/MIL-53(Al), **(d)** [BMIM][CF_3SO_3]/MIL-53(Al), **(e)** [BMIM][SbF_6]/MIL-53(Al), **(f)** [BMIM][NTf_2]/MIL-53(Al) at 50 and 12.5 K× magnifications.

X-Ray Diffraction (XRD) Spectroscopy

Table S4. XRD peak positions of pristine MIL-53(Al) and IL/MIL-53(Al) composites.

Sample	**Related XRD peaks (°)**					
MIL-53(Al)	8.8	9.4	12.3	15.2	17.7	26.6
[BMIM][BF_4]/MIL-53(Al)	8	8.5	11.4	14.9	17.0	26.7
[BMIM][PF_6]/MIL-53(Al)	8.7	9.9	10.5	15.2	17.7	26.6
[BMIM][CF_3SO_3]/MIL-53(Al)	8.9	9.1	10.3	15.3	17.7	26.6
[BMIM][SbF_6]/MIL-53(Al)	9.7	9.9	10.3	15.8	18.6	26.6
[BMIM][NTf_2]/MIL-53(Al)	8.7	9	10.6-11.1	15.1	17.4	26.6

Thermal Gravimetric Analysis (TGA)

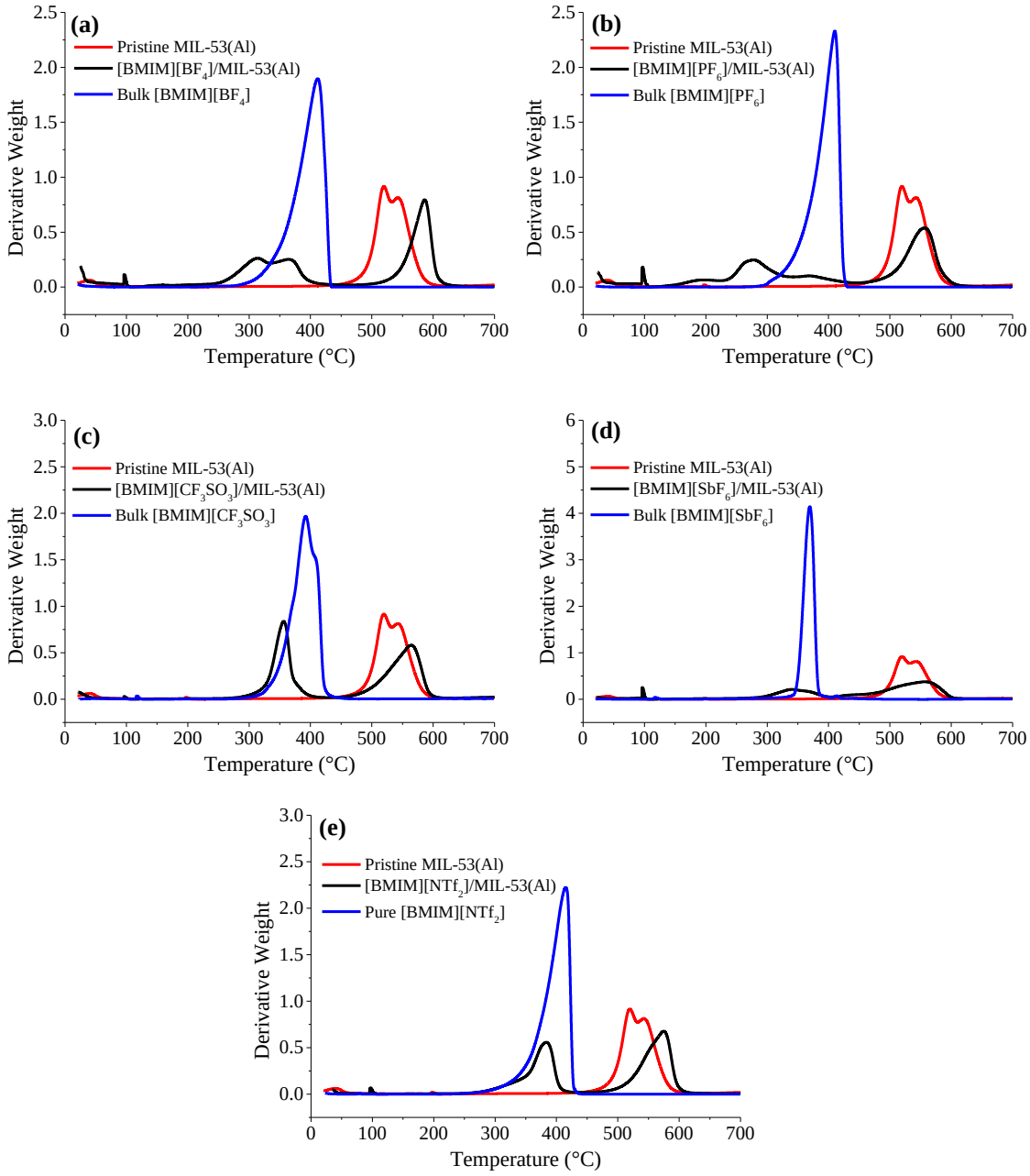

Figure S4. Derivative weight change of pristine MIL-53(Al), bulk ILs, and IL/MIL-53(Al) composites, where the IL is **(a)** [BMIM][BF_4], **(b)** [BMIM][PF_6], **(c)** [BMIM][CF_3SO_3], **(d)** [BMIM][SbF_6], and **(e)** [BMIM][NTf_2].

Table S5. T'_{onset} values of pristine MIL-53(Al), bulk ILs: [BMIM][BF_4], [BMIM][PF_6], [BMIM][CF_3SO_3], [BMIM][SbF_6] and [BMIM][NTf_2], and composites: [BMIM][BF_4]/MIL-53(Al), [BMIM][PF_6]/MIL-53(Al), [BMIM][CF_3SO_3]/MIL-53(Al), [BMIM][SbF_6]/MIL-53(Al), and [BMIM][NTf_2]/MIL-53(Al).

MOF	IL	T'_{onset} of pure IL (°C)	T'_{onset} of composite (°C)	% wt. loss of bulk IL (700 °C)	% wt. loss of composite (700 °C)
			484		61.8
	[BMIM][BF_4]	350	253	99.7	66.1
MIL-	**[BMIM][PF_6]**	358	233	99.7	64.6
53(Al)	**[BMIM][CF_3SO_3]**	342	326	97	70.9
	[BMIM][SbF_6]	350	285	89	62.1
	[BMIM][NTf_2]	357	342	99.8	68.7

Fourier Transform Infrared (FTIR) Spectroscopy

All IL/MIL-53(Al) composites showed the characteristic IR features of their ILs in the region of 3200-2800 cm^{-1}. The data indicate red or blue shifts on the peak positions of these features from their corresponding positions in bulk materials. For instance, the symmetric stretching vibration of C(4)HC(5)H, ν_{ss}(C(4)HC(5)H), of the imidazolium ring showed red shifts of 3 and 7 cm^{-1} for [BMIM][BF_4]/MIL-53(Al) and [BMIM][PF_6]/MIL-53(Al), respectively. ν_{ss}(C(4)HC(5)H) of [BMIM][CF_3SO_3]/MIL-53(Al) showed a blue shift of 4 cm^{-1}, while for [BMIM][SbF_6]/MIL-53(Al) and [BMIM][NTf_2]/MIL-53(Al) the shifts were in the spectral resolution. The most acidic H atom in the $[BMIM]^+$ is bonded to the C atom between two N atoms in the imidazolium ring. Therefore, ν(C(2)−H) vibration is a good indicator of the interactions between anion and cation, and IL and MOF. For [BMIM][BF_4]/MIL-53(Al) and [BMIM][PF_6]/MIL-53(Al), ν(C(2)−H) red-shifted by 5 and 6 cm^{-1}, respectively, while it was red-shifting by 8 cm^{-1} for both [BMIM][SbF_6]/MIL-53(Al) and [BMIM][NTf_2]/MIL-53(Al). The ν(C(2)−H) vibration red-shifted from 3115 to 3101 cm^{-1} in [BMIM][CF_3SO_3]/MIL-53(Al) composite. A similar behavior of ν(C(4)HC(5)H) and ν(C(2)−H) vibrations of IL/MIL-53(Al) composites might be reasonable as both C(4)HC(5)H and C(2)−H are involved in H bonding between anion and cation, and both are the indicators of interionic interactions.[5] As given in Table S6, $[BMIM]^+$ originated IR spectra of IL/MIL-53(Al) composites demonstrated that IL−MOF interaction depends on the type of IL. Anion related peaks could help to understand the anion-cation and IL−MOF interactions in a clearer way. Antisymmetric stretching vibrations of $[BF_4]^-$ and $[PF_6]^-$, ν_{as}(BF_4) and ν_{as}(PF_6), red-shifted by 8 and 6 cm^{-1} in [BMIM][BF_4]/MIL-53(Al) and [BMIM][PF_6]/MIL-53(Al), respectively. In the composites prepared by incorporating [BMIM][BF_4] and [BMIM][PF_6] into MIL-53(Al), the corresponding ν(C(2)−H) bands red-shifted, indicate the lengthening of the bond between C(2) and H. This change suggests that hydrogen bonding between anion and cation gets stronger as consistent with the literature.[6] This strengthening in the hydrogen bond between anion and cation weakens the ν_{as}(BF_4) and ν_{as}(PF_6) vibrations. MOF-originated IR peaks of these composites showed that ν_{ss}(Al−O−Al), ν_{as}(Al−O−Al), δ(O−H), and μ_2(O−H) red-shifted by 6, 17, 14, and 4 cm^{-1} in [BMIM][BF_4]/MIL-53(Al) and 4, 19, 7, and 6 cm^{-1} in [BMIM][PF_6]/MIL-53(Al), respectively. On the other hand, the position of ν(C−C), which is in the organic linker part of the MOF, did not change within the spectral resolution of the measurements. These findings demonstrate that [BMIM][BF_4] and [BMIM][PF_6] interact with the aluminum backbone and bridging (O−H) group of the MIL-53(Al), while they do not

interact with the organic linker side. In the case of [BMIM][CF_3SO_3]/MIL-53(Al), $\nu_{ss}(SO_3)$ and $\nu_{as}(SO_3)$, red-shifted by 5 and 6 cm^{-1}, and ν(C(4)HC(5)H) and ν(C(2)−H) showed blue and red shifts of 4 and 14 cm^{-1}, respectively. (Al−O−Al) vibrations, ν(C−C) and δ(C−C−C) did not show any significant shifts, while μ_2(O−H) vibration was slightly red-shifting by 3 cm^{-1}. These findings might indicate that with a blue shift in ν(C(2)−H), the C(2)−H bond shortens in length and hydrogen bonding between anion and cation gets weaker. Red shifts in (SO_3) vibrations can be the result of IL−MOF interactions through (SO_3) side of the anion, and consequently, the (CF_3) side of the anion gets stronger as indicated by a blue shift in $\nu_{as}(CF_3)$. [BMIM][SbF_6]/MIL-53(Al) and [BMIM][NTf_2]/MIL-53(Al) reveal a similar behavior: their ν(C(4)HC(5)H), μ_2(O−H), ν(C−C), δ(C−C−C), and ν_{ss}(Al−O−Al) remained the same within the spectral resolution of the measurements. The position of ν(C(2)−H) red-shifted from 3122 cm^{-1} to 3114 cm^{-1} in both composites. For the anion side of [BMIM][SbF_6]/MIL-53(Al), ν(SbF_6) slightly blue-shifted from 658 cm^{-1} to 661 cm^{-1}. Similarly, in the anion side of [BMIM][NTf_2]/MIL-53(Al), the peaks positions for ν_{as}(S−N) and $\nu_{as}(CF_3)$ do not change much. ν(C−S) blue-shifted by 11 cm^{-1}, while ν_{ss}(S−N), $\nu_{ss}(SO_2)$, and $\nu_{as}(SO_2)$ were red-shifting by 4, 3, and 7 cm^{-1}, respectively. These results might indicate that anions of [BMIM][SbF_6] and [BMIM][NTf_2] interact with MIL-53(Al) and share their electrons with the MOF. This electron sharing causes a strengthening in (Sb−F) and (C−S) bond strengths as indicated by blue shifts in ν(SbF_6) and ν(C−S).

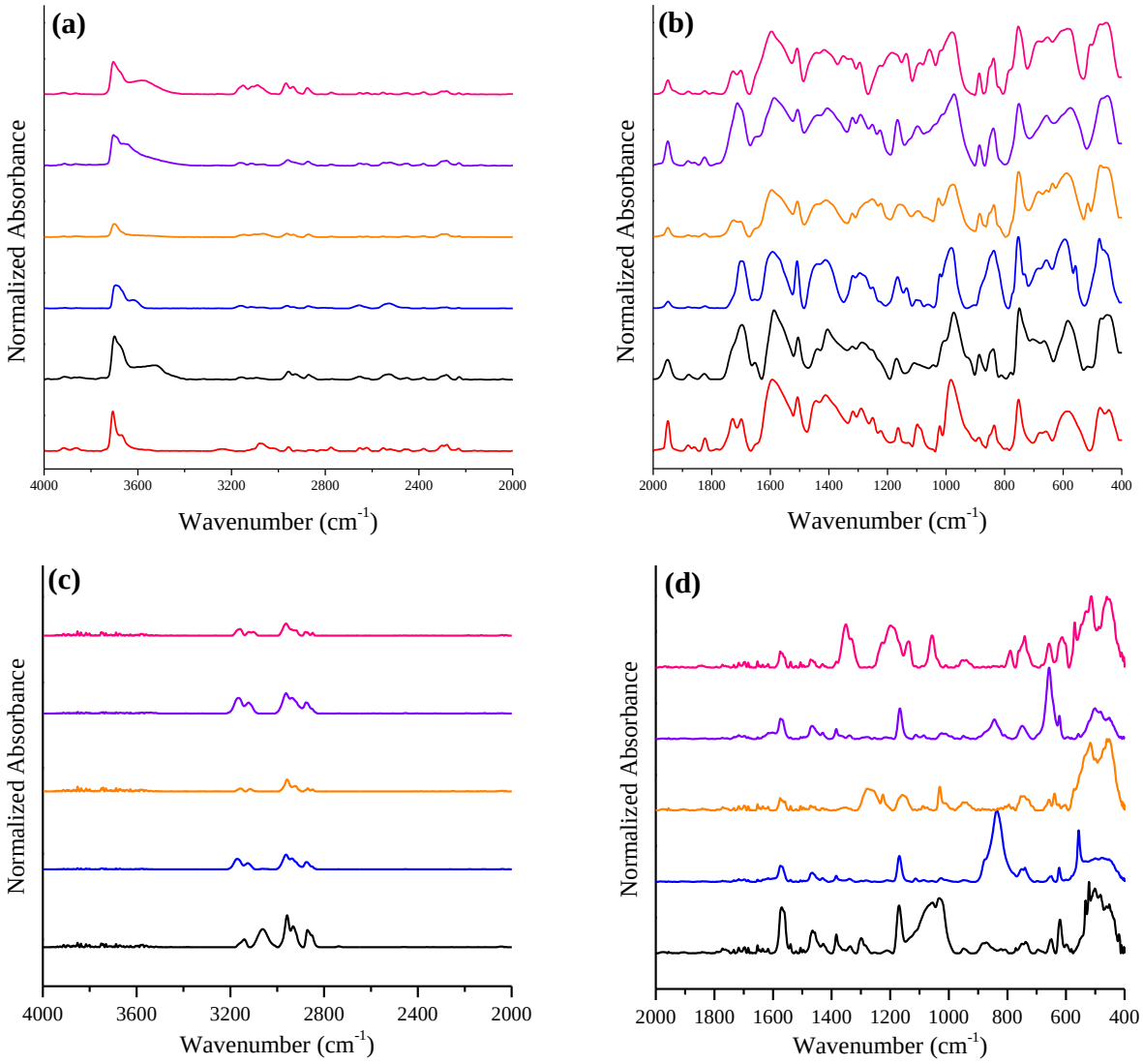

Figure S5. IR spectra of pristine MIL-53(Al) and IL/MIL-53(Al) composites in the region of **(a)** 4000-2000 cm^{-1} and **(b)** 2000-400 cm^{-1}, and of bulk ILs in the region of **(c)** 4000-2000 cm^{-1} and **(d)** 2000-400 cm^{-1}. Color code: red, pristine MIL-53(Al); black, [BMIM][BF_4]; blue, [BMIM][PF_6]; orange, [BMIM][CF_3SO_3]; violet, [BMIM][SbF_6]; pink, [BMIM][NTf_2].

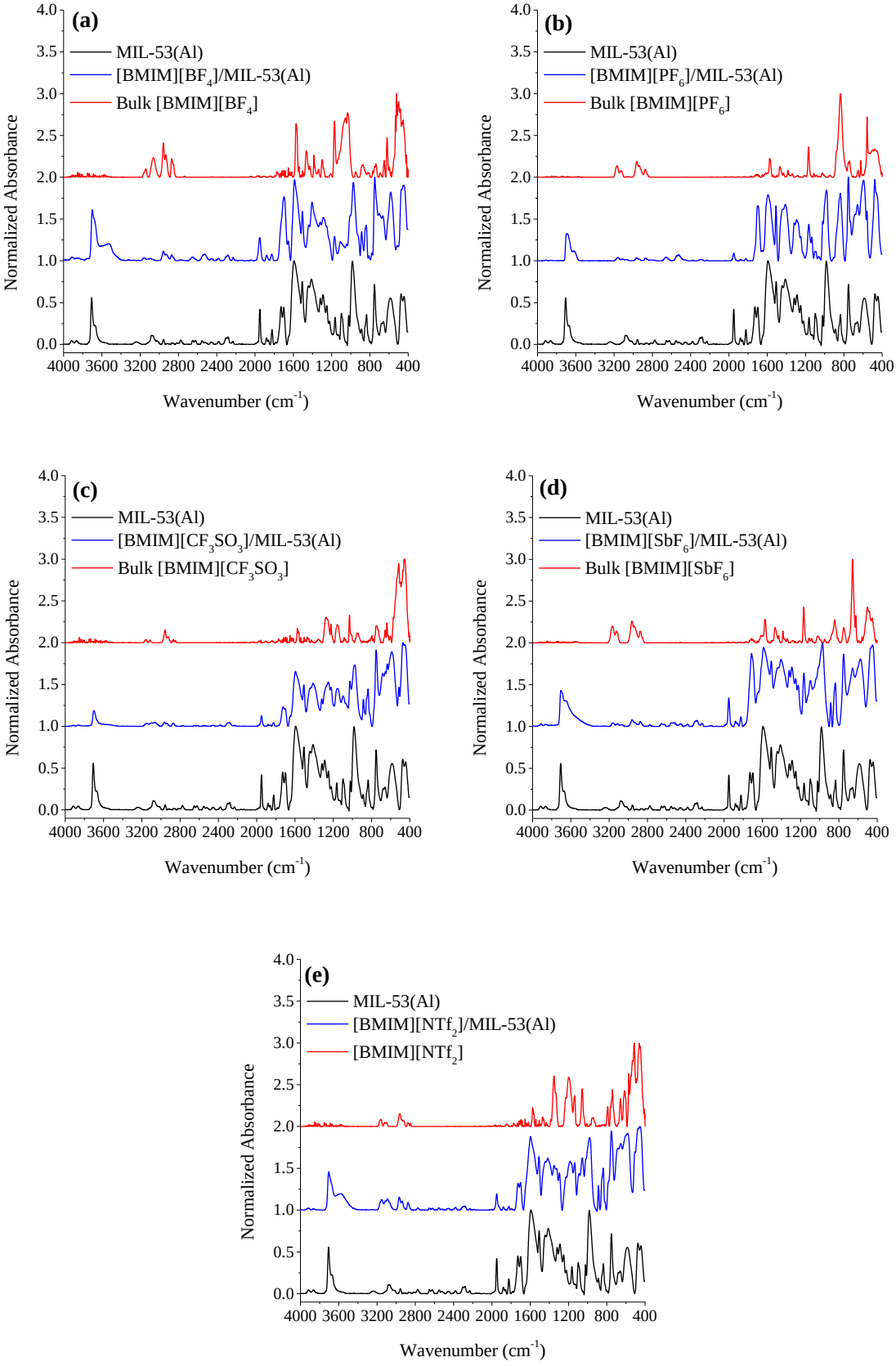

Figure S6. IR spectra comparison of pristine MIL-53(Al), bulk ILs and IL/MIL-53(Al) composites between 4000-400 cm^{-1}, where the IL is **(a)** [BMIM][BF_4], **(b)** [BMIM][PF_6], **(c)** [BMIM][CF_3SO_3], **(d)** [BMIM][SbF_6], and **(e)** [BMIM][NTf_2].

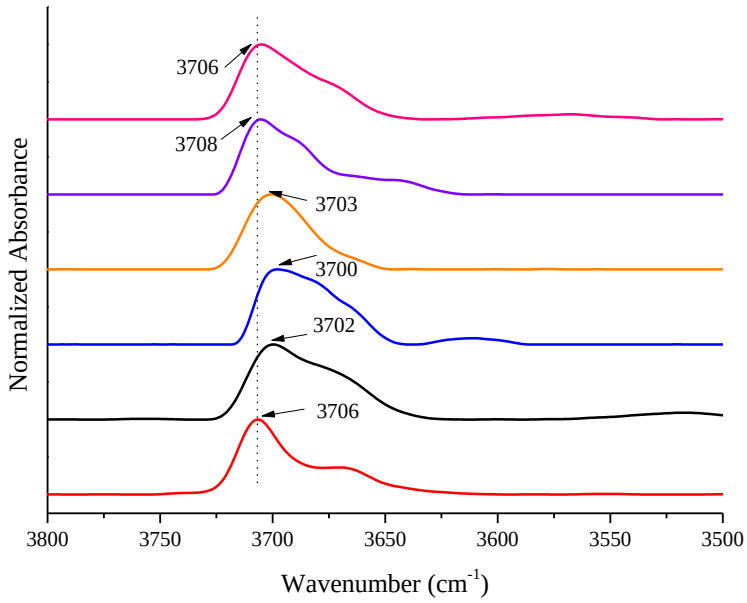

Figure S7. IR spectra showing μ_2(O−H) vibrations of pristine MIL-53(Al) and IL/MIL-53(Al) composites around 3700 cm^{-1}. From bottom to top: pristine MIL-53(Al), [BMIM][BF_4]/MIL-53(Al), [BMIM][PF_6]/MIL-53(Al), [BMIM][CF_3SO_3]/MIL-53(Al), [BMIM][SbF_6]/MIL-53(Al), and [BMIM][NTf_2]/MIL-53(Al), respectively.

Table S6. Assignments for the vibrational IR bands of MIL-53(Al).

Vibrational Band Assignment	Position of the peak (cm^{-1})
μ_2(O−H)	3706
ν_{sym}(Al−O−Al)	658
ν_{as}(Al−O−Al)	681
δ(C−C−C) + δ(O−C−O)	853
δ(O−H)	980
	992
δ(C−C−C) + δ(C−H)	1024
ν_{sym}(O−C−O)	1414
ν(C−C) + δ(C−H)	1505

Table S7. Assignments for the vibrational IR bands of bulk ILs.

Vibrational Band Assignment	Position of the peak (cm^{-1})				
	[BMIM] [BF_4]	**[BMIM] [PF_6]**	**[BMIM] [CF_3SO_3]**	**[BMIM] [SbF_6]**	**[BMIM] [NTf_2]**
ν_{ss}(C(4)HC(5)H)	3173	3170	3158	3167	3169
ν(C(2)−H)	3125	3124	3115	3122	3122
ν_{ss}(N)CH_3	2965	2963	2958	2966	2963
ν_{FR}(CH_3)	2933	2936	2924	2938	2935
ν_{ss}(CH_3)	2862	2850	2849	2867	2848
ν_{as}(CH_2)	2876	2874	2869	2879	2881
	751[a]	736[c]	1280[d]	658[g]	740[h]
	1021[b]	836[c]	1225[d]		791[i]
	1169[b]	557[c]	1257[e]		1058[j]
			1161[f]		1137[k]
					1130[l]
					1167[m]

[a]ν_{ss}(BF_4), [b]ν_{as}(BF_4), [c]ν_{as}(PF_6), [d]ν_{ss}(SO_3), [e]ν_{as}(SO_3), [f]ν_{as}(CF_3), [g]ν(SbF_6), [h]ν(C−S), [i]ν_{ss}(S−N), [j]ν_{as}(S−N), [k]ν_{ss}(SO_2), [l]ν_{as}(SO_2) and [m]ν_{as}(CF_3).

Table S8. Assignments of MOF originated IR shifts of IL/MIL-53(Al) composites. Table is color mapped according to the magnitude of the red or blue shifts. For the convenience, $[BMIM]^+$ in the names of ILs are not mentioned in the table.

	$[BF_4]$ /MIL-53(Al)	**$[PF_6]$ /MIL-53(Al)**	**$[CF_3SO_3]$ /MIL-53(Al)**	**$[SbF_6]$ /MIL-53(Al)**	**$[NTf_2]$ /MIL-53(Al)**
μ_2(O−H)	-4	-6	-3	2	0
ν_{sym}(Al−O−Al)	-6	-4	0	-3	-2
ν_{as}(Al−O−Al)	-17	-19	3	12	9
δ(C−C−C) + δ(O−C−O)	-4	-3	-2	-3	-1
δ(O−H)	-13	-6	-9	-10	-12
	-14	-7	-5	-2	-14
δ(C−C−C) + δ(C−H)	-11	-1	3	-6	-2
ν_{sym}(O−C−O)	-7	-6	-6	-6	1
ν(C−C) + δ(C−H)	-1	3	2	1	3

Table S9. Assignments of IL originated IR shifts of IL/MIL-53(Al) composites. Table is color mapped according to the magnitude of the red or blue shifts. For the convenience, $[BMIM]^+$ in the names of ILs are not mentioned in the table.

	$[BF_4]$ /MIL-53(Al)	**$[PF_6]$ /MIL-53(Al)**	**$[CF_3SO_3]$ /MIL-53(Al)**	**$[SbF_6]$ /MIL-53(Al)**	**$[NTf_2]$ /MIL-53(Al)**
ν_{ss}(C(4)HC(5)H)	-4	-8	4	1	-1
ν(C(2)−H)	-5	-6	-11	-8	-8
ν_{ss}(N)CH_3	-6	1	6	-6	5
ν_{FR}(CH_3)	-8	-2	10	-8	2
ν_{ss}(CH_3)	-11	9	-1	-11	21
ν_{as}(CH_2)	-5	0	0	-5	-2
	2[a]	-6[c]	-5[d]	3[g]	11[h]
	-8[b]	0[c]	-6[d]		-4[i]
	0[b]	0[c]	-1[e]		2[j]
			6[f]		-3[k]
					-7[l]
					-1[m]

[a]$\nu_{ss}(BF_4)$, [b]$\nu_{as}(BF_4)$, [c]$\nu_{as}(PF_6)$, [d]$\nu_{ss}(SO_3)$, [e]$\nu_{as}(SO_3)$, [f]$\nu_{as}(CF_3)$, [g]$\nu(SbF_6)$, [h]ν(C−S), [j]ν_{ss}(S−N), [k]ν_{as}(S−N), [l]$\nu_{as}(SO_2)$, and [m]$\nu_{as}(CF_3)$.

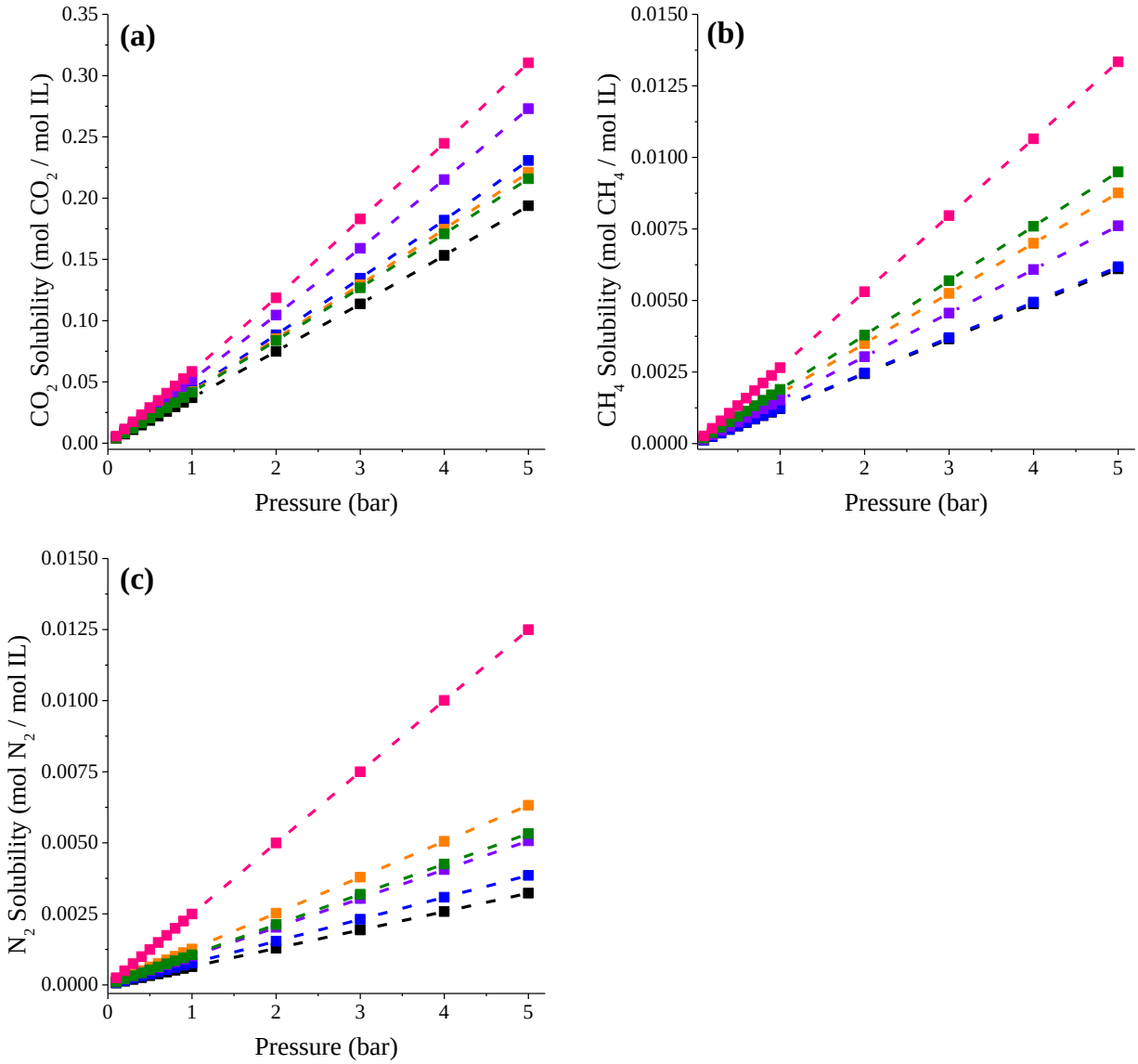

Figure S8. (a) CO_2, **(b)** CH_4, and **(c)** N_2 solubilities of bulk ILs calculated by COSMO-RS. Color code: black, [BMIM][BF_4]; blue, [BMIM][PF_6]; orange, [BMIM][CF_3SO_3]; violet, [BMIM][SbF_6]; olive, [BMIM][$MeSO_4$]; pink, [BMIM][NTf_2].

Gas Adsorption Analyses

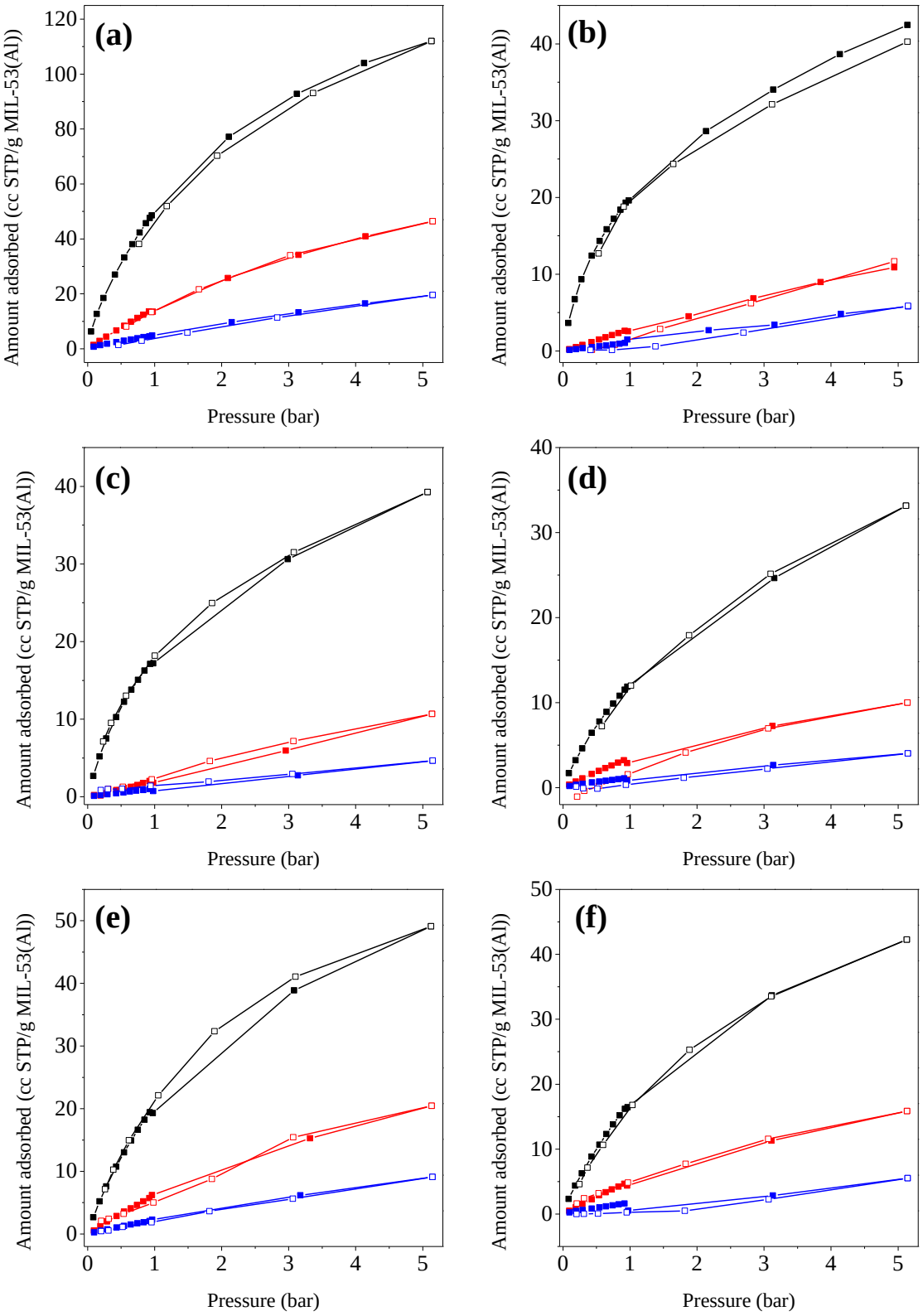

Figure S9. Gas adsorption-desorption isotherms of (a) pristine MIL-53(Al), (b) [BMIM][BF_4]/MIL-53(Al), (c) [BMIM][PF_6]/MIL-53(Al), (d) [BMIM][CF_3SO_3]/MIL-53(Al), (e) [BMIM][SbF_6]/MIL-53(Al), and (f) [BMIM][NTf_2]/MIL-53(Al). Color code: black, CO_2; red, CH_4; blue, N_2. Filled (empty) squares represent adsorption (desorption).

Table S10. Fitting parameters of dual-site Langmuir model* for pristine MIL-53(Al) and IL/MIL-53(Al) composites.

Sample	Gas	q_1 (cc/g)	k_1 (1/mbar)	q_2 (cc/g)	k_2 (1/mbar)	R^2
Pristine MIL-53(Al)	CO_2	161.337	0.358	7.756	13.599	0.999
	CH_4	101.860	0.163	1.321×10^{-14}	0.688	0.999
	N_2	0.629	12.289	101.563	0.045	0.999
[BMIM][BF_4]/ MIL-53(Al)	CO_2	70.618	0.113	17.782	2.483	0.999
	CH_4	18.344	0.102	207.489	4.720×10^{-3}	0.999
	N_2	41.829	0.015	40.203	0.015	0.997
[BMIM][PF_6]/ MIL-53(Al)	CO_2	581.187	6.055×10^{-3}	28.715	1.154	0.999
	CH_4	7466.430	2.938×10^{-4}	8.916×10^{-4}	1.527×10^{-8}	0.999
	N_2	0.382	1.191	2165.180	4.073×10^{-4}	0.999
[BMIM][CF_3SO_3]/ MIL-53(Al)	CO_2	11.215	0.989	100.075	0.035	0.998
	CH_4	964.945	4.025×10^{-4}	8.829	0.301	0.999
	N_2	0.477	3.942	2075.560	3.573×10^{-4}	0.997
[BMIM][SbF_6]/ MIL-53(Al)	CO_2	77.429	0.238	10.307	1.647	0.999
	CH_4	37.695	0.146	12.650	0.146	0.999
	N_2	42.569	0.056	0.149	4.146	0.999
[BMIM][$MeSO_4$]/ MIL-53(Al)	CO_2	33.579	0.859	302.378	1.009×10^{-2}	0.999
	CH_4	540.923	1.321×10^{-3}	317.435	5.671×10^{-3}	0.998
	N_2	4242.480	1.738×10^{-4}	0.057	1.498	0.983
[BMIM][NTf_2]/ MIL-53(Al)	CO_2	0.945	15.491	71.001	0.329	0.999
	CH_4	875.965	5.034×10^{-4}	29.674	0.193	0.999
	N_2	1.000×10^{4}	7.662×10^{-5}	1.484	1.668	0.984

*Dual-site Langmuir model is as follows,

$$n\,(P) = q_1 \times \frac{k_1 \times P}{1 + k_1 \times P} + q_2 \times \frac{k_2 \times P}{1 + k_2 \times P}$$

where P is the pressure of bulk gas at equilibrium with the adsorbed phase. q_1 and q_2 represent the saturation capacity on sites #1 and #2, while k_1 and k_2 are the affinity constants.

Table S11. Fitting parameters for virial-type thermal adsorption equation* for CO_2, CH_4 and N_2 isotherms measured at 10 and 20 °C for [BMIM][PF_6]/MIL-53(Al) composite material.

Fit Parameters	**MIL-53(Al)**			**[BMIM][PF_6]/MIL-53(Al)**		
	CO_2	CH_4	N_2	CO_2	CH_4	N_2
a_0	-4213.780	-1890.370	-1504.709	-4365.530	-1345.460	-1216.670
a_1	98.790	-13.505	10	55.650	-13.530	-14.490
a_2	-1.750	0.034	-0.971	4.450×10^{-2}	-0.930	-0.930
a_3	9.090×10^{-3}	0	0	-3.640×10^{-2}	0	0
a_4	9.570×10^{-6}	0	0	3.500×10^{-4}	0	0
a_5	-6.460×10^{-8}	0	0	4.500×10^{-8}	0	0
b_0	11.000	3.768	3.236	12.560	3.970	2.780
b_1	-0.280	0.056	0.066	-0.270	0.120	0.510
b_2	5.280×10^{-3}	0	0	6.820×10^{-3}	0	0
b_3	-2.820×10^{-5}	0	0	-3.700×10^{-5}	0	0

*Virial-type thermal adsorption equation:

$$\ln P = \ln N + \frac{1}{T}\sum_{i=0}^{5} a_i N^i + \sum_{i=0}^{3} b_i N^i$$

where N is the gas uptake, P is the pressure of gas at equilibrium, T is the temperature and, a_i and b_i are the fitting parameters of the equation.

Isosteric heat of adsorption (Q_{st}) is calculated using the equation below;

$$Q_{st} = -R\sum_{i=0}^{5} a_i N^i$$

where N is the gas uptake, R is the gas constant, and a_i is fitting parameters obtained by fitting the virial-type thermal adsorption equation.

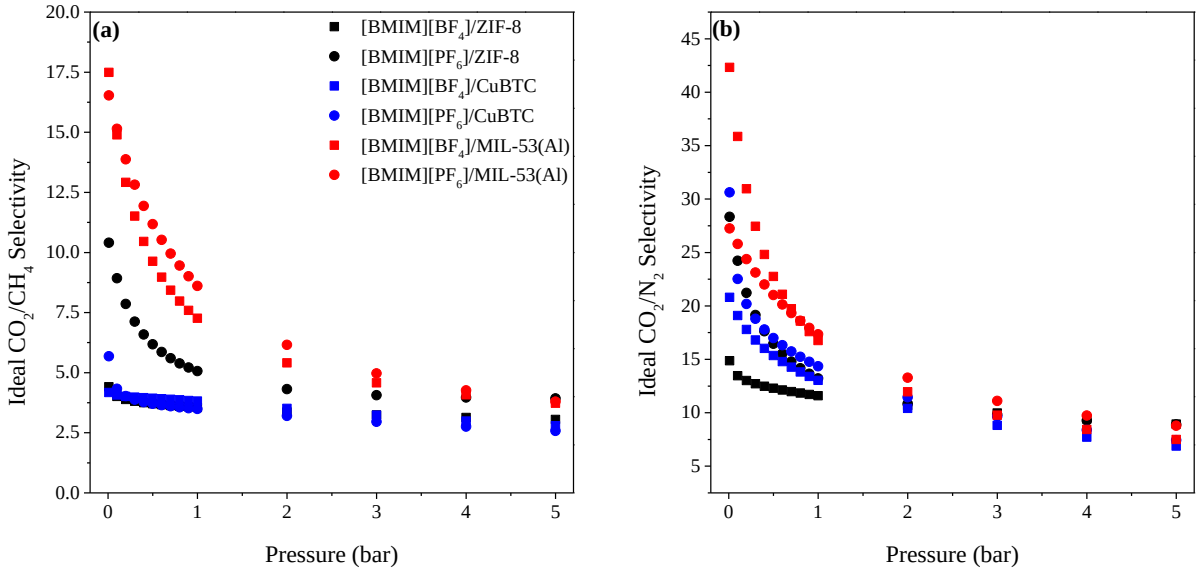

Figure S10. Ideal (a) CO_2/CH_4 and (b) CO_2/N_2 selectivities of [BMIM][BF_4]-incorporated and [BMIM][PF_6]-incorporated ZIF-8,[2,9] CuBTC,[1,8] and MIL-53(Al) composites as a function of pressure.

Characterization of [BMIM][$MeSO_4$]/MIL-53(Al)

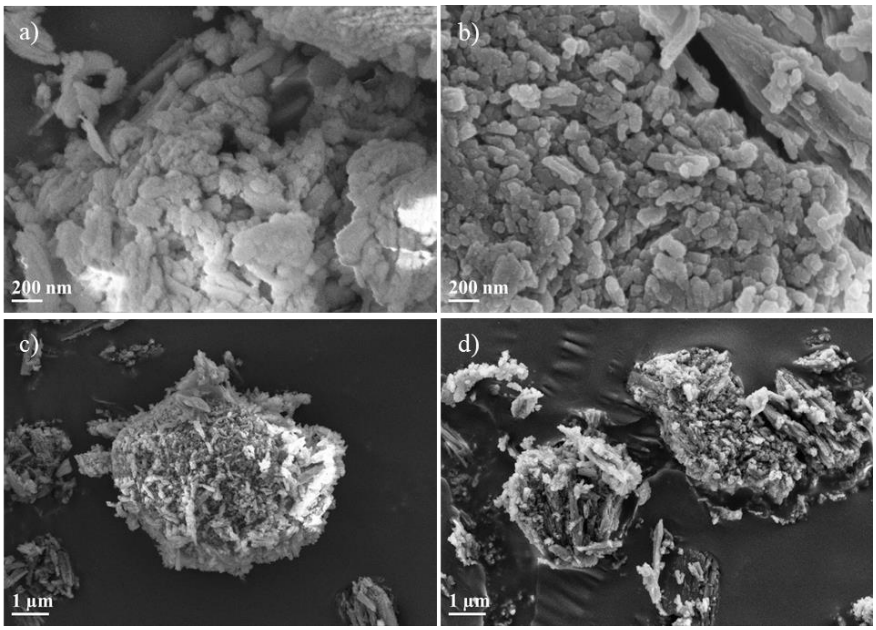

Figure S11. SEM micrographs of (a and c) MIL-53(Al) and (b and d) [BMIM][$MeSO_4$]/MIL-53(Al) at a magnification of 100 K× (a, b) and 25 K× (c, d). Reprinted with the permission from Ref.[7] Copyright 2019 Wiley-VCH.

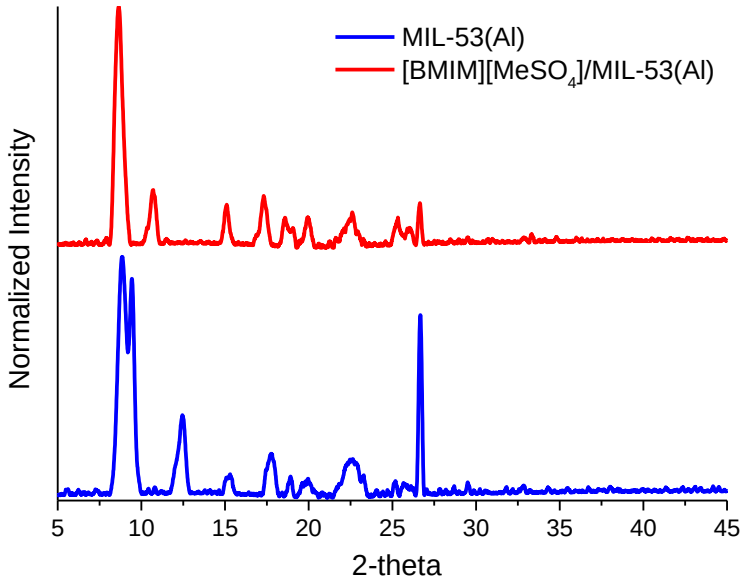

Figure S12. X-ray diffraction patterns of MIL-53(Al) (blue) and [BMIM][MeSO4]/MIL-53(Al) (red). Reprinted with the permission from Ref.[7] Copyright 2019 Wiley-VCH.

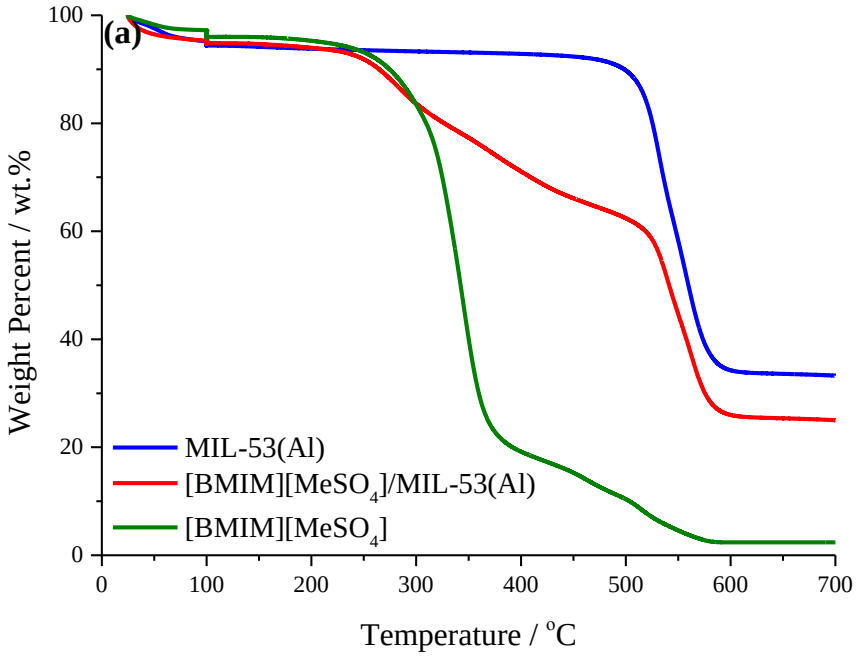

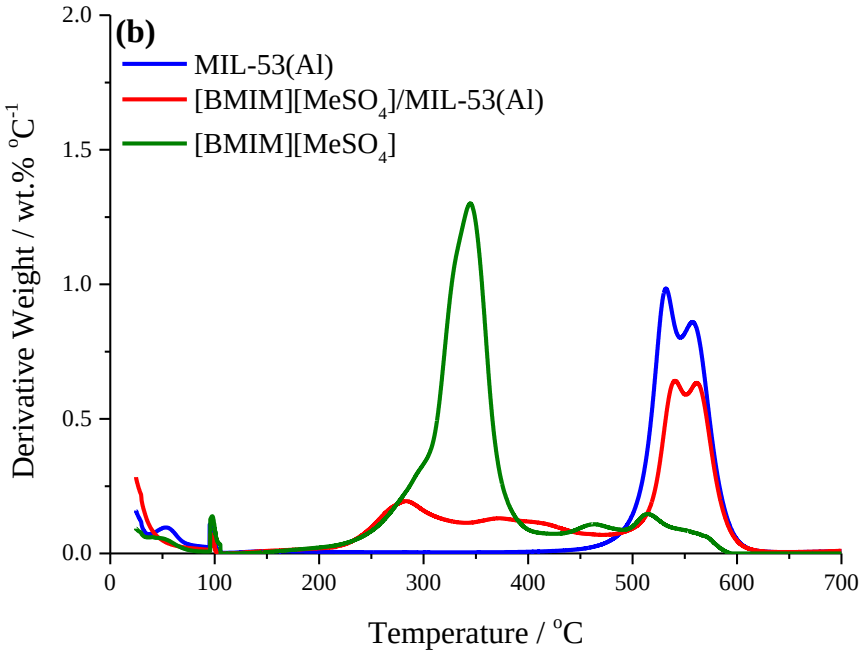

Figure S13. (a) TGA and (b) DTG curves of pristine MIL-53(Al) (blue), bulk [BMIM][MeSO4] (green), and [BMIM][MeSO4]/MIL-53(Al) (red) samples. Reprinted with the permission from Ref.[7] Copyright 2019 Wiley-VCH.

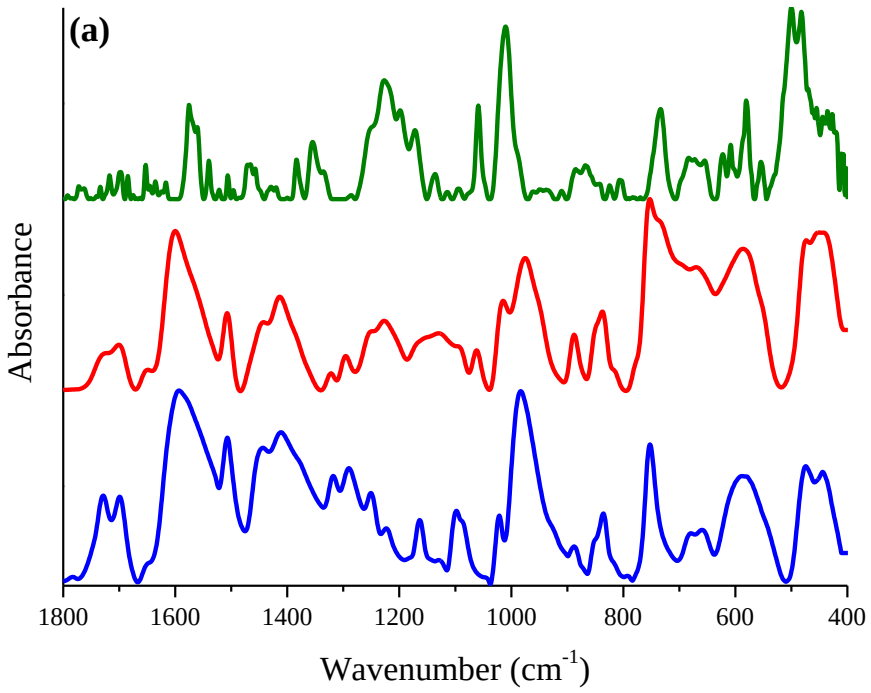

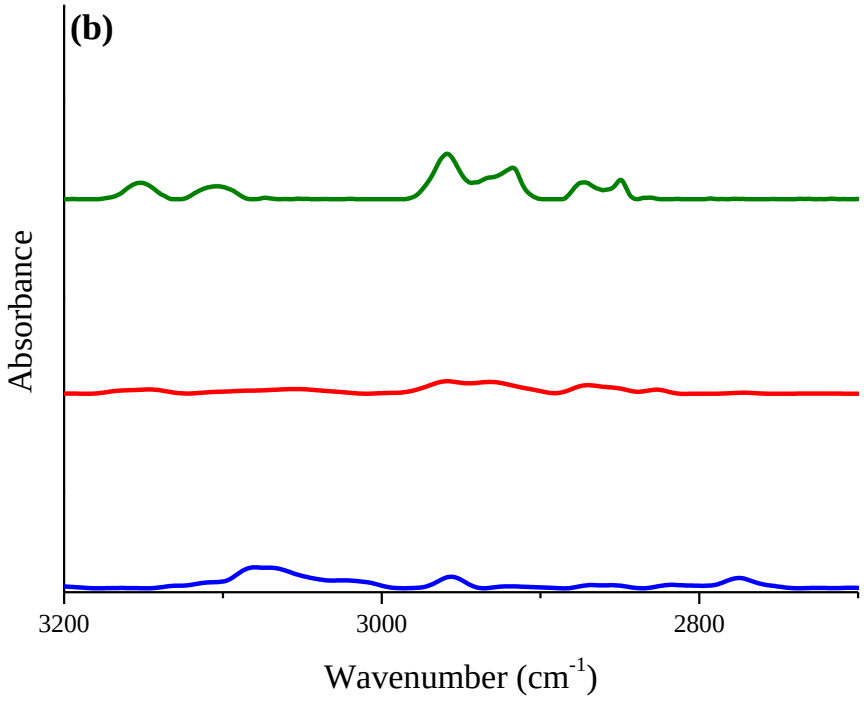

Figure S14. FTIR spectra of pristine MIL-53(Al) (blue), bulk [BMIM][$MeSO_4$] (green), and [BMIM][$MeSO_4$]/MIL-53(Al) (red) samples between (a) 1800 and 400 cm^{-1}, and (b) 3200 and 2700 cm^{-1}. Reprinted with the permission from Ref.[7] Copyright 2019 Wiley-VCH.

References

[1] V. Nozari, M. Zeeshan, S. Keskin, A. Uzun, *CrystEngComm* **2018**, *20*, 7137-7143.

[2] F. P. Kinik, C. Altintas, V. Balci, B. Koyuturk, A. Uzun, S. Keskin, *ACS Appl. Mater. Interfaces* **2016**, *8*, 30992-31005.

[3] F. H. Allen, *Acta Cryst.* **2002**, *B58*, 380-388.

[4] T. Loiseau, C. Serre, C. Huguenard, G. Fink, F. Taulelle, M. Henry, T. Bataille, G. Férey, *Chem. Eur. J.* **2004**, *10*, 1373-1382.

[5] K. Fumino, A. Wulf, R. Ludwig, *Angew. Chem. Int. Ed.* **2008**, *47*, 3830-3834.

[6] K. Nakamoto in *Infrared and Raman Spectra of Inorganic and Coordination Compounds*, 4th Ed., Wiley Interscience, New York, USA, **1986**.

[7] H. Kulak, H. M. Polat, S. Kavak, S. Keskin, A. Uzun, *Energy Technol.* **2019**, Doi: 10.1002/ente.201900157.

[8] K. B. Sezginel, S. Keskin, A. Uzun, *Langmuir* **2016**, *32*, 1139-1147.

[9] B. Koyuturk, C. Altintas, F. P. Kinik, S.Keskin, A. Uzun, *J. Phys. Chem. C* **2017**, *121*, 10370-10381.